

Chirality | Hot Paper |

Controlling Mirror Symmetry Breaking and Network Formation in Liquid Crystalline Cubic, Isotropic Liquid and Crystalline Phases of Benzil-Based Polycatenars

Tino Reppe, Silvio Poppe, and Carsten Tschierske*^[a]

Abstract: Spontaneous development of chirality in systems composed of achiral molecules is important for new routes to asymmetric synthesis, chiral superstructures and materials, as well as for the understanding of the mechanisms of emergence of prebiotic chirality. Herein, it is shown that the 4,4'-diphenylbenzil unit is a universal transiently chiral bent building block for the design of multi-chained (polycatenar) rod-like molecules capable of forming a wide variety of helically twisted network structures in the liquid, the liquid crystalline (LC) and the crystalline state. Single polar substituents at the apex of tricatener molecules support the formation of

the achiral (racemic) cubic double network phase with $la\bar{3}d$ symmetry and relatively small twist along the networks. The combination of an alkyl chain with fluorine substitution leads to the homogeneously chiral triple network phase with $I23$ space group, and in addition, provides a mirror symmetry broken liquid. Replacing F by Cl or Br further increases the twist, leading to a short pitch double gyroid $la\bar{3}d$ phase, which is achiral again. The effects of the structural variations on the network structures, either leading to achiral phases or chiral conglomerates are analyzed.

Introduction

Dynamic self-assembled networks of any kind represent the fundamental basis of open-end development in complex systems. For example, neural networks are responsible for the development of the brain and consciousness, chemical networks are the basis of metabolism, data networks for information technology and so on.^[1–4] Bicontinuous cubic (Cub_{bi}) liquid crystalline phases can be considered as soft self-assembled networks, which have attracted a lot of interest for conducting and photonic materials, as matrices for protein crystallization and as templates for sol–gel syntheses.^[5,6] Recently, these fluid networks were recognized to be responsible for transmission and amplification of chirality in fluid systems, and thus could provide a new potential route to prebiotic chirality.^[7,8] Cub_{bi} phases are known for different types of small molecular^[9–11] or polymeric^[12] amphiphiles, either in aqueous systems (lyotropic phases)^[6,13] or as pure compounds (thermotropic phases).^[9,10,14] Amphiphilicity can be based on any intramolecular difference

of intermolecular interactions leading to nano-segregation of incompatible units,^[15] like polar and nonpolar^[11] or rod-like polycyclic aromatic cores and flexible chains.^[16–27]

In the Cub_{bi} phases of rod-like compounds the double gyroid phase with space group $la\bar{3}d$ involving two networks with three-way junctions (see Figure 1 a)^[6,9] and a more complex triple network structure with larger lattice parameters and $I23$ space group, also involving exclusively three-way junctions, were observed.^[9,22,23] The networks are separated by the alkyl chains organized around the infinite minimal surfaces located in the middle between them.^[28] The $I23^{*k}$ -type Cub_{bi} phase is exceptional, not only as it is the only presently known Cub_{bi} phase with triple network structure, it was recently also found to be inherently chiral^[29–31] and the discovery of this supramolecular chirality provided an improved general understanding of the cubic phases formed by rod-like molecules. The most prominent are the 4'-*n*-alkyloxy-3'-nitrophenyl-4-carboxylic acids (ANBCs)^[32] and the 1,2-bis(4'-*n*-alkyloxybenzoyl)hydrazines (BABHs),^[33,34] both involving hydrogen bonding and having only one alkyl chain at each end, and the so-called polycatenar compounds, having more than only two terminal chains (Scheme 1).^[35–37] In the Cub_{bi} phases of these compounds the rod-like cores are organized in the networks with the long axes perpendicular or slightly tilted to the local net direction. The clashing of the bulky molecular peripheries leads to a helical twist along the networks (Figure 1 d), which is transmitted by the junctions to the macroscopic scale.^[29a,38] The $la\bar{3}d$ phase with only two enantiomorphous networks with opposite handedness is macroscopically achiral (Figure 1 a).^[39] In the triple network phase this degeneracy is broken by the third network (Figure 1 b) and a synchronization of the helix

[a] T. Reppe, Dr. S. Poppe, Prof. Dr. C. Tschierske
Institute of Chemistry
Martin Luther University Halle-Wittenberg
Kurt-Mothes-Straße 2, 06120 Halle (Germany)
E-mail: carsten.tschierske@chemie.uni-halle.de

Supporting information and the ORCID identification number(s) for the author(s) of this article can be found under:
<https://doi.org/10.1002/chem.202002869>.

© 2020 The Authors. Published by Wiley-VCH GmbH. This is an open access article under the terms of Creative Commons Attribution NonCommercial License, which permits use, distribution and reproduction in any medium, provided the original work is properly cited and is not used for commercial purposes.

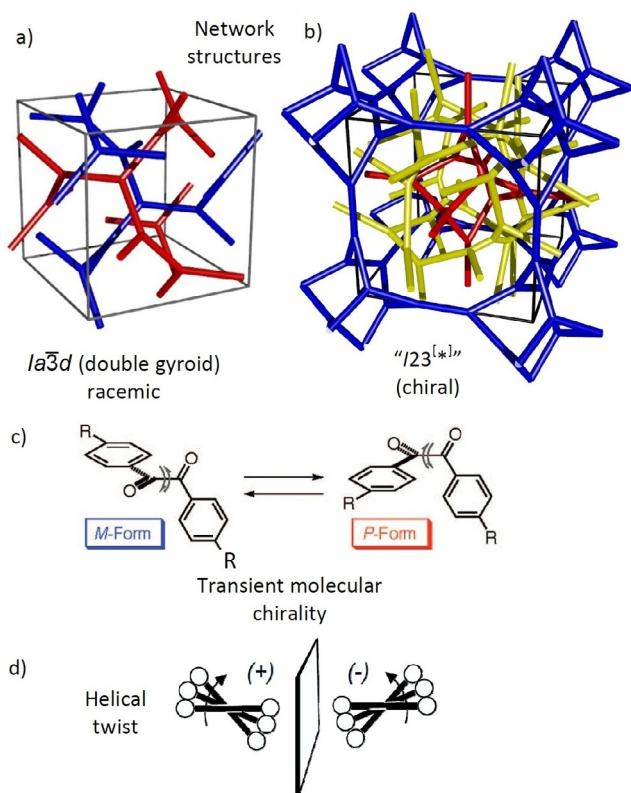
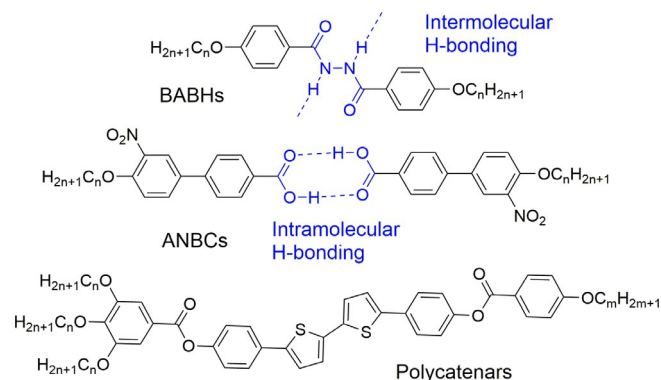


Figure 1. Schematics showing the networks of a) the $Cub_{bi}/Ia\bar{3}d$ phase and b) the triple network $I23^{[*]}$ phase; c) shows the transient chirality of the benzil unit and d) the development of the helical twist by clashing of bulky end groups attached to the cores.^[44] The polyaromatic cores are located in the networks and aligned almost perpendicular to the network directions, the continuum between them is filled by the terminal alkyl chains; b) was reproduced from ref. [31] by permission of The Royal Society of Chemistry.



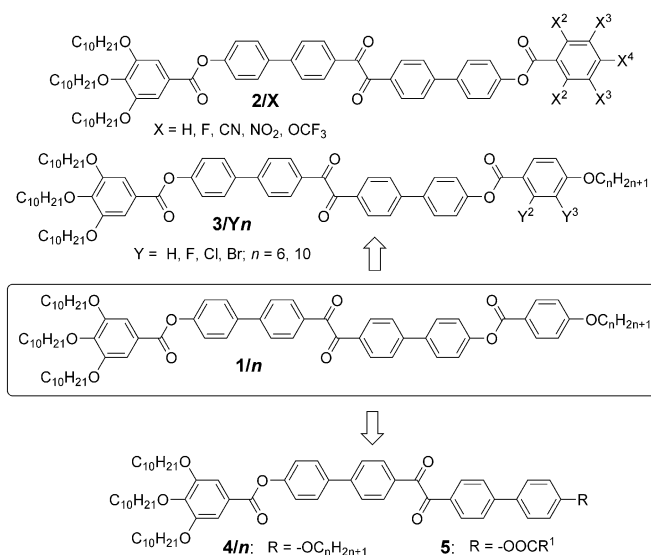
Scheme 1. Structures of the BABH and ANBC based rod-like hydrogen bonded molecules and supramolecules, and an example of a polycatenar mesogens forming Cub_{bi} phases.

sense between the interwoven networks leads to uniform chirality ($I23^{[*]}$ phase, the spontaneous chirality is indicated by $^{[*]}$).^[40–43]

Notably, there are two distinct type of $Ia\bar{3}d$ phases, occurring on either side of the $I23^{[*]}$ phase, a long pitch (low twist) $Ia\bar{3}d_{(L)}$ and a short pitch (high twist) $Ia\bar{3}d_{(S)}$ phase, leading to the phase sequence $Ia\bar{3}d_{(L)}/I23^{[*]}/Ia\bar{3}d_{(S)}$ with growing twist be-

tween the molecules along the networks.^[44–46] In previous work we have shown that these rod-like molecules do not only form mirror symmetry broken cubic phases, mirror symmetry breaking is in some cases even observed in the adjacent isotropic liquid phases ($Iso_1^{[*]}$), forming liquid conglomerates.^[45,47] These $Iso_1^{[*]}$ phases usually occur besides one of the Cub_{bi} phases and therefore they are considered as liquid network phases.^[38,44]

The 4,4'-diphenylbenzil derived polycatenars **1/n** (Scheme 2) with a torsion of the $O=C=O$ bond,^[48] represent transiently chiral molecules,^[38] which were recently shown to even form a sequence of three mirror symmetry broken mesophases, thus transferring chirality from the isotropic liquid ($Iso_1^{[*]}$) via the liquid crystalline ($Cub_{bi}/I23^{[*]}$) to the crystalline state ($Cr_{Iso}^{[*]}$).^[44] Herein we expand this class of compounds by investigating the importance of the core length (compounds **4/n** and **5** in Scheme 2) and the effect of polar substituents in lateral position (compounds **3/Yn**) or at one end (at the apex, compounds **2/X** in Scheme 2) on the self-assembly, network formation and spontaneous mirror symmetry breaking in the liquid state.



Scheme 2. Structures of the compounds under investigation, for details of the structures, see Tables 1–4.

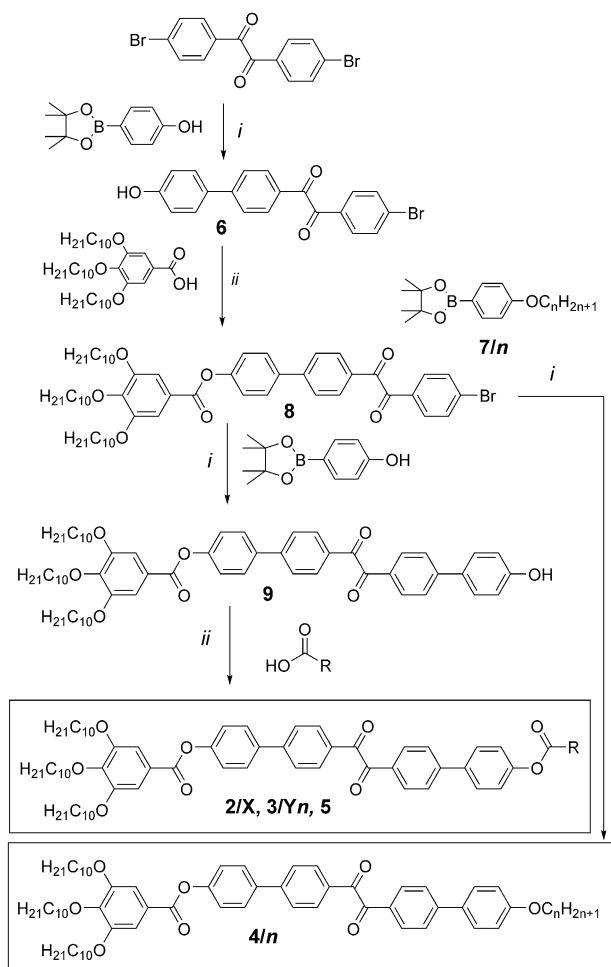
Experimental Section

Synthesis

The target compounds were synthesized according to Scheme 3. Compounds **2/X**, and **5** were obtained by acylation of the phenol **9**^[44] using the experimental procedures given in the Supporting Information (SI). The alkoxy compounds **4/n** were synthesized from the aryl bromide **8** by Suzuki cross-coupling with 4-alkoxyphenylboronic acid pinacol esters **7/n**.

Investigations

Investigations of the compounds were performed by polarizing optical microscopy between crossed and slightly uncrossed polarizers (POM), differential scanning calorimetry (DSC) and X-ray scattering



Scheme 3. Synthesis of the benzil-based compounds 2–5. Reagents and conditions: (i) THF, sat. NaHCO_3 solution, $[\text{Pd}(\text{PPh}_3)_4]$, reflux; (ii) SOCl_2 , abs. pyridine, DCM, DMAP, 25°C .

(small angle X-ray scattering = SAXS and wide angle scattering = WAXS) with the instrumentation described in the Supporting Information. The transition from the isotropic liquid state to the Cub_{bi} phases on cooling was identified by an increase of viscosity associated with a small DSC peak (Figure S1) while the phase remains optically isotropic (Figure 2b,e). In the X-ray scattering patterns of the Cub_{bi} phases there are several small angle scatterings besides the diffuse wide angle scattering. The diffuse character of the wide angle scattering with a maximum around $d = 0.45$ nm (Figures S3b and S4b) confirms the LC state having no fixed positions of the individual molecules. The small angle scattering positions can be indexed either to (211) and (220) of a $1a\bar{3}d$ lattice or to (321), (400) and (420) of the $I23^{[*]}$ lattice (Tables S2 and S3). Figures S3 and S4 show representative SAXS patterns of these two cubic phase types. Additional confirmation of the cubic phase type was gained from optical investigation under a polarizing microscope between polarizers slightly rotated by a few degrees out of the exactly 90° twisted orientation where only the $I23^{[*]}$ phase shows a conglomerate of chiral (dark and bright) domains which invert their brightness by changing the twist direction of the analyzer (see Figure 2a–c) whereas the $1a\bar{3}d$ phase does not, and therefore is achiral (Figure 2c–f).^[29a] In a similar way the achiral isotropic melted state (Iso, Iso) is distinguished from the conglomerates formed by the mirror symmetry broken $\text{Iso}_1^{[*]}$ phase. The non-cubic LC phases were indicated by their typical birefringent textures as observed by POM between crossed polarizers and confirmed by SAXS investigation (see Section 3.3 and Table S4).

Results and Discussion

The series of tetracatenar compounds 4/n

In the series of compounds 4/n with a shorter 5-ring core, incorporating one benzoate unit less than the 6-ring compounds 1/n, the homologues with a chain length between $n = 14$ and 18 form a monotropic Cub_{bi} phase on cooling, whereas all other homologues have exclusively crystalline phases

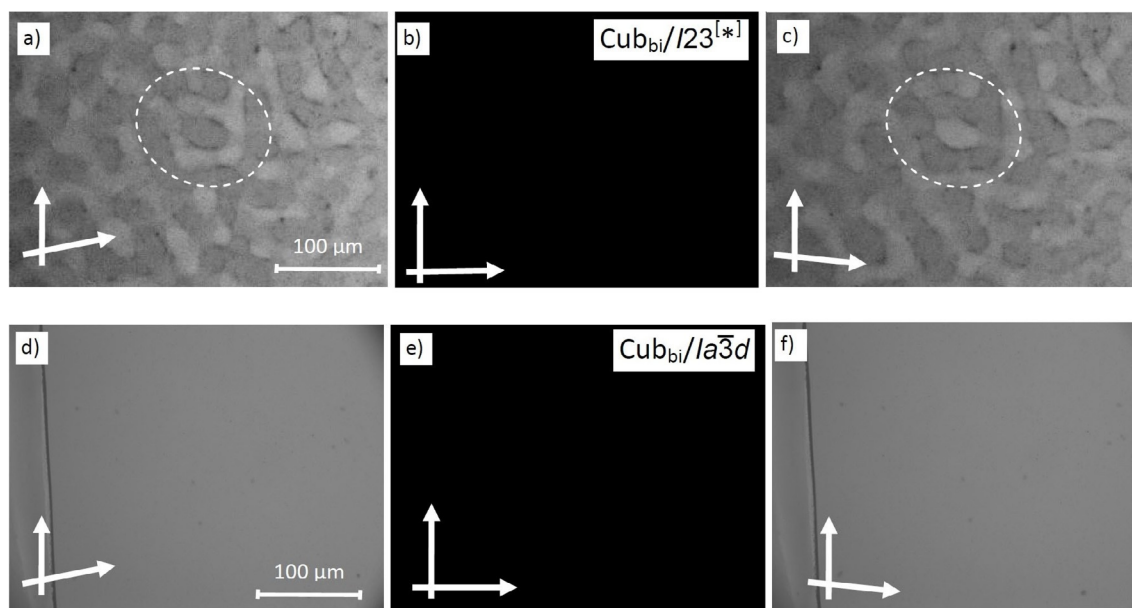
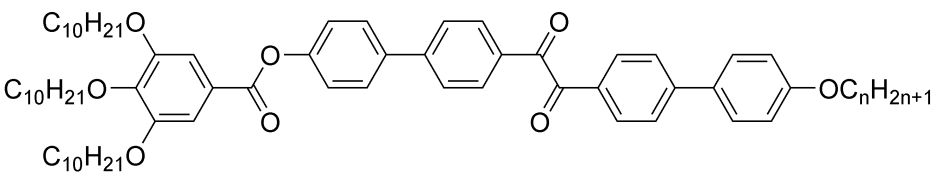


Figure 2. POM images as observed between crossed (middle) and slightly uncrossed polarizers (left, right) for a–c) the $I23^{[*]}$ phase of 1/10 at 105°C as obtained after cooling from the $\text{Iso}_1^{[*]}$ phase and d–f) the achiral $1a\bar{3}d$ phase of $3^2\text{Br}6$ at 70°C as observed on cooling from Iso.

Table 1. Phase transitions of the homologous series of compounds **4/n** measured on heating and cooling (10 K min⁻¹).^[a]


Compound	<i>n</i>	Heating: <i>T</i> [°C] [ΔH in kJ mol ⁻¹]	Cooling: <i>T</i> [°C] [ΔH in kJ mol ⁻¹]
4/4	4	Cr 82 [48.0] Iso	Iso 45 [-19.5] Cr
4/6	6	Cr 91 [64.2] Iso	Iso 42 [-21.7] Cr
4/8	8	Cr 96 [51.4] Iso	Iso 63 [-45.2] Cr
4/10 ^[44]	10	Cr 102 [54.7] Iso	Iso 81 [-53.3] Cr
4/12	12	Cr 80 [66.5] Iso	Iso 57 [-49.4] Cr
4/14	14	Cr 82 [78.3] Iso	Iso 69 [-6.5] Iso ₁ , 49 [-1.3] Cub/ <i>la</i> 3 <i>d</i> 31 [-6.0] Cr ^[c]
4/16	16	Cr 83 [75.3] Iso	Iso 70 [-6.1] Iso ₁ , 55 [-1.9] Cub/ <i>la</i> 3 <i>d</i> 31 [-2.5] Cr ^[c]
4/18	18	Cr 84 [92.3] Iso	Iso 66 [-19.9] ^[b] Iso ₁ , 56 [-1.3] Cub/ <i>la</i> 3 <i>d</i> 37 [-7.7] Cr ^[c]
4/20	20	Cr 86 [110.0] Iso	Iso 66 [-83.8] Cr

[a] DSC peak temperatures on heating at 10 K min⁻¹. Abbreviations: Cr = crystalline solid, Iso = achiral isotropic liquid; Cub/*la*3*d* = achiral bicontinuous cubic phase; though the direct assignment of the *la*3*d* type was not possible, based on the large chain length a *la*3*d*_(s) type appears more likely; for DSCs of compounds **4/14**–**4/18**, see Figures 3 and S1a–c. [b] Transition is accompanied by partial crystallization. [c] Partial crystallization.

(Table 1). Even for these three compounds, due to rapid crystallization, the phase transitions can only be recorded on cooling by DSC and optical investigations, whereas crystallization takes place during the exposure time of attempted XRD investigations. The assignment of these cubic phases to the *la*3*d* space group is therefore only based on optical investigations, indicating the absence of chiral domains in the isotropic mesophases with high viscosity.

Only for **4/14** and **4/16** the transition from Iso to Cub_{bi}/*la*3*d* takes place without partial crystallization on cooling. The most interesting feature of these compound is an additional transition in the isotropic liquid state before the transition to the cubic phase (Table 1, Figures 3 and Figure 1a–c). On cooling compound **4/14**, as example, a broad feature occurs in the DSC traces in the temperature range of the isotropic liquid phase, indicating a liquid state polyamorphism (liquid–liquid

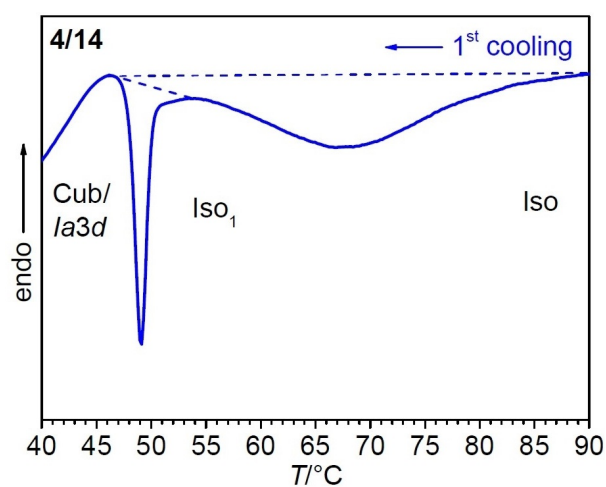


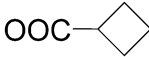
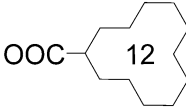
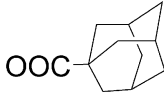
Figure 3. DSC of compound **4/14** showing the Iso–Iso₁–Cub_{bi}/*la*3*d* transition ranges; full heating and cooling scans are shown in Figure S1 a, the DSCs of **4/16** and **4/18** are shown in Figure S1 b,c.

transitions, see Figure 3).^[9b,38,44,46,49a] The additional sharp peak at the transition to the cubic phase is associated with a sudden change from fluidity to viscoelasticity. The majority of the enthalpy of this Iso–Iso₁–Cub_{bi} transition is involved in this broad feature (6–7 kJ mol⁻¹) which is interpreted as a growth of aggregates which fuse to a network structure and continuously increases network connectivity (Iso₁ phase),^[38a,44, 49a] being in line with recent results of ¹H-NMR diffusion and relaxation studies.^[49b] At a certain degree of network connectivity, the long range cubic lattice composed of two interwoven gyroid networks with three way junctions is formed. This is indicated by a sharp peak with small enthalpy (1.3–1.9 kJ mol⁻¹). There is no indication of any mirror symmetry breaking in the Iso₁ phase range and therefore we assume a similar *la*3*d*-like network with three way junctions, but without long range order for the structure of the achiral Iso₁ phase. As the Iso₁ phase flows under gravity like any other ordinary liquid, the network must be highly dynamic and we consider it as a kind of percolated network liquid.^[44] The very broad Iso–Iso₁ transition is interpreted as a continuous growth process fusing the cybotactic clusters to dynamic networks.^[38a,44] Though this broad DSC feature was also observed for compound **4/18**, the Iso–Iso₁ transition is in this case accompanied by a partial crystallization, as indicated by the changed shape and larger enthalpy of this broad transition (Figure S1 c).

Tetracatenar compound **5/n** with an acyl chain and tricate-nar compounds **5** with cyclic units at the apex

Attempts to widen the cubic range of compounds **4/n** by using acyloxy chains (**5/12**) or alicyclic and polycyclic units (compounds **5/c4**, **5/c12** and **5/Ad**) instead of alkyloxy chains failed (see Table 2), though in the series of polycatenar dicarboxylates of 5,5'-diphenyl-2,2'-dithiophene (Scheme 1) a significant mesophases stabilizing effect of these cycloaliphatic units was found.^[45] As shown in Table 2 all these compounds **5** are

Table 2. Phase transitions of compounds **5** on heating and cooling (DSC at 10 Kmin⁻¹).

Compound	R	T [°C] [ΔH in kJ mol ⁻¹]
4/12 ^(b)	OC ₁₂ H ₂₅	H: Cr 80 [66.5] Iso C: Iso 57 [-49.4] Cr
5/12	OOC ₁₂ H ₂₅	H: Cr 87 [53.4] Iso C: Iso 65 [-45.4] Cr
5/c4		H: Cr 104 [67.0] Iso C: Iso 45 [-19.8] Cr
5/c12		H: Cr 106 [66.8] Iso C: Iso <20 Cr
5/Ad		H: Cr 79 [35.5] Iso C: Iso <20 Cr

crystalline solids, some of them can be supercooled even down to room temperature without mesophase formation before the onset of crystallization. It appears that the capability of the non-symmetric 5-ring tetracatenars **4** for mesophase formation is limited to only few examples with long aliphatic chains. Therefore, the focus of the following work is on compounds **2** and **3** with a polyaromatic core involving six benzene rings.

Tricatenar compounds with polar substituents at the apex

We expanded the structure of the tetracatenar six-ring compounds **1/n** either by introduction of halogens in lateral positions of the apex or by replacing the alkoxy chain at the apex by polar electron withdrawing substituents (tricate nar compounds **2/X**). As shown in Table 3, electron withdrawing groups, especially CN and NO₂, lead to compounds with wide ranges of LC phases, most probably due to increasing polar core-core interactions between the electron deficit aromatics as well as by donor-acceptor interactions with the electron-donor-substituted trialkoxylated ends in an antiparallel packing.^[45,50] **2/CN** and **2/NO₂** show an enantiotropic phase sequence Iso-Iso₁-SmA-Cub_{bi} on cooling. The SmA phases were confirmed by their typical fan-like textures with extinctions parallel to the directions of analyzer and polarizer (Figure 4a,b), and the optically isotropic appearance of their homeotropic aligned samples (see insets in Figure 4a,b), thus confirming optically uniaxial non-tilted SmA phases. The SAXS patterns show only one sharp scattering with $d=5.5$ (**2/CN**) or $d=5.3$ nm (**2/NO₂**, see Table S4), being a bit larger than the molecular lengths $L_{\text{mol}}=4.5$ and 4.6 nm, respectively, measured for the most extended conformation of space filling models (Figure 5a). Thus, it can be concluded that an almost fully interca-

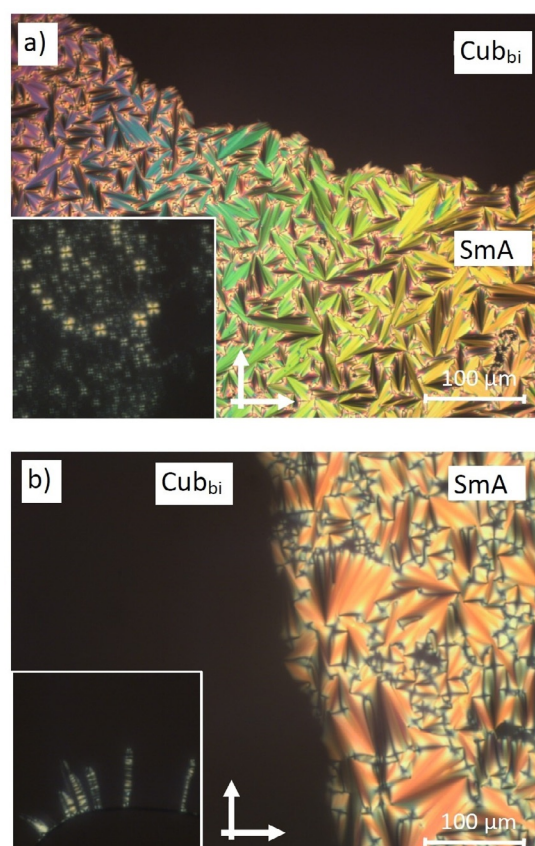
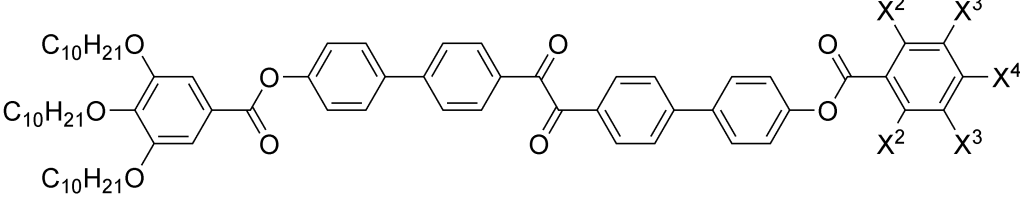


Figure 4. Textures of a) **2/CN** at $T=147$ °C and b) **2/NO₂** at $T=167$ °C in planar aligned samples showing the growth of the Cub_{bi}/*1a3d* phase (dark area) into the fan textures of the birefringent SmA phases on cooling; the insets show the homeotropic textures of the SmA phases at 150 and 170 °C, respectively; the arrows indicate the orientation of polarizer and analyzer.

Table 3. Phase transitions, lattice parameters (a_{cub}) and twist angles between the molecules in neighboring rafts (Φ) in the Cub_{bi} phases of compounds **2/X**.^[a]


Compound	X ⁴	X ³	X ²	T [°C] [ΔH in kJ mol ⁻¹]	n_{raft}	a_{cub} [nm] (Φ /°)
1/0 ^[44]	H	H	H	H: Cr 126 [52.2] Iso; C: Iso 110 [27.3] Cr	–	–
1/1 ^[44]	OMe	H	H	H: Cr 127 [36.3] Iso; C: Iso 115 [36.4] Cr	–	–
1/2 ^[44]	OEt	H	H	H: Cr 120 [37.9] $la\bar{3}d_{\text{(L)}}$ 127 [1.8] Iso ₁ 135 [1.9] Iso C: Iso 133 [–1.3] Iso ₁ 121 [–0.2] Iso ₁ ^[b] 110 [–0.3] $la\bar{3}d_{\text{(L)}}$ 105 [–31.3] Cr	4.9	12.9 (6.9)
1/14 ^[44]	OC ₁₄ H ₂₉	H	H	H: Cr 108 [44.1] $la\bar{3}d_{\text{(S)}}$ 135 [2.9] Iso ₁ 138 [7.0] Iso C: Iso 136 [–3.1] Iso ₁ 129 [–1.2] Col _{hex} 125 [–0.4] $la\bar{3}d_{\text{(S)}}$ 42 [–16.9] Cr _{Iso} < 20 Cr	3.2	11.3 (7.9)
2/F	F	H	H	H: Cr 126 [26.5] Iso; C: Iso 110 [27.3] Cr	–	–
2/CN	CN	H	H	H: Cr 145 [25.0] $la\bar{3}d_{\text{(L)}}$ 165 [1.2] SmA ^[b] 176 [1.0] Iso ₁ 183 Iso C: Iso 178 [–2.9] Iso ₁ 173 [–0.8] SmA 145 [–0.9] $la\bar{3}d_{\text{(L)}}$ 124 [–34.4] Cr H: Cr 149 [38.9] $la\bar{3}d_{\text{(L)}}$ 181 [2.0] SmA ^[c] 187 [1.7] Iso ₁ 193 [2.5] Iso C: Iso 190 [–3.0] Iso ₁ 184 [–1.5] SmA 167 [–1.8] $la\bar{3}d_{\text{(L)}}$ 130 [–41.0] Cr	4.6	12.4 (7.2)
2/NO₂	NO ₂	H	H	H: Cr 123 [24.9] $la\bar{3}d_{\text{(L)}}$ 135 [2.2] Iso ₁ 143 [4.0] Iso C: Iso 141 [–2.4] Iso ₁ 126 [–1.6] $la\bar{3}d_{\text{(L)}}$ 115 [–25.3] Cr	3.8	11.3 (7.9)
2/F₃	F	F	H	H: Cr 123 [28.1] $la\bar{3}d_{\text{(L)}}$ 130 [2.9] Iso ₁ 138 [3.4] Iso C: Iso 134 [–3.4] Iso ₁ 121 [–2.2] $la\bar{3}d_{\text{(L)}}$ 103 [–26.4] Cr	3.6	10.9 (8.2)
2/F₅	F	F	F	H: Cr 103 [39.7] $la\bar{3}d_{\text{(L)}}$ 112 [2.0] Iso ₁ 123 [5.2] Iso C: Iso 118 [–7.7] Iso ₁ 100 [–1.6] $la\bar{3}d_{\text{(L)}}$ 84 [–43.1] Cr	3.5	10.8 (8.3)

[a] DSC peak temperatures on heating/cooling (H/C) at 10 K min⁻¹; n_{raft} = number of molecules in the cross section of the networks, calculated for rafts with a height of 0.45 nm; for details of the calculations see Table S5; a_{cub} = cubic lattice parameter; $\Phi(la\bar{3}d)$ = twist between adjacent molecules (rafts), calculated according to $\Phi(la\bar{3}d) = 70.5^\circ / (0.354 a_{\text{cub}} / 0.45 \text{ nm})$; ^[29a] for DSCs, see Figures 7 and S1 and for X-ray scattering data Tables S2–S5 and Figures S3 and S4; for the Iso–Iso₁ transitions, representing broad features the maxima of the features are given, the complete temperature ranges are listed in Table S1; abbreviations: SmA = non-tilted lamellar (smectic A) phase; $la\bar{3}d_{\text{(L)}}$ = long pitch (small Φ) $la\bar{3}d$ phase; $la\bar{3}d_{\text{(S)}}$ = short pitch (large Φ) $la\bar{3}d$ phase; for the other abbreviations, see Table 1; [b] $d = 5.5$ nm; [c] $d = 5.3$ nm.

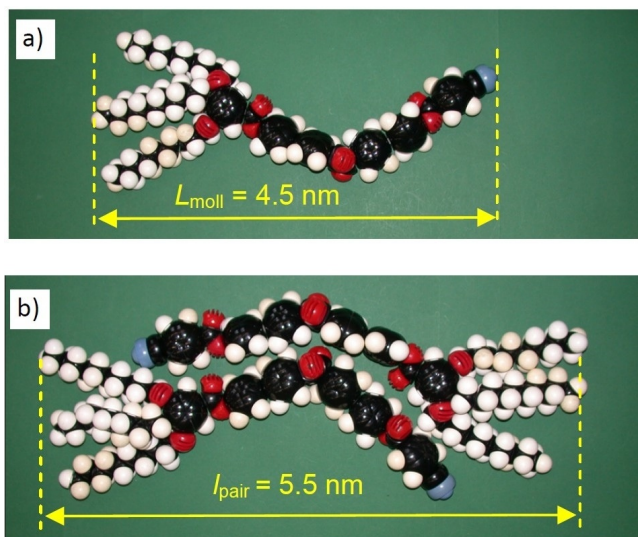


Figure 5. a) Space filling models of compound **2/CN** and b) its antiparallel pair with fully intercalated aromatic cores.

lated antiparallel organization of the molecules in the layers, providing a layer distance of 5.5 nm, is present (Figure 5b).

In the cubic phases two main small angle scattering peaks are observed which can be indexed to (211) and (220) of a $la\bar{3}d$ lattice; the calculated lattice parameters a_{cub} are 12.4 nm for **2/CN** (155 °C) and 12.1 nm for **2/NO₂** (160 °C, see Tables 3, S2 and S4). According to $d_{\text{rod}} = \sqrt{3} \times a_{\text{cub}} / 4$ the distance between the two networks is $d_{\text{rod}} = 5.4$ and 5.2 nm, respectively (see Table S5). This distance corresponds to the separation of the minimal surface and is similar to the layer distances measured in the adjacent SmA phases. This is in line with a non-tilted fully intercalated organization of the polyaromatic rods in the networks (Figure 5b). The cubic phase stability (and mesophases stability in general) of the 4-substituted compounds **2/X** grows in the order $X = \text{F} < \text{OCF}_3 < \text{CN} < \text{NO}_2$ with rising Hammett constants of the substituents ($\sigma_m + \sigma_p$ for $\text{F} = 0.4$; $\text{OCF}_3 = 0.7$; $\text{CN} = 1.2$ and $\text{NO}_2 = 1.5$).^[51]

Increasing degree of fluorination at the apex has a similar effect as CN/NO₂ substitution. Though the monofluorinated compound **2/F** does not show any LC phase, probably due to its rapid crystallization on cooling, taking place already at 110 °C, the further increase of the number of fluorines induces cubic phases. This works for aromatic fluorination^[52] (**2/F₃** and **2/F₅**) as well as for the fluorination of the OCH₃ group (compound **2/OCF₃**, see Table 3), though there is a competition with the simultaneously growing steric effect of fluorination.

All compounds **2/X** with polar substituents form exclusively the achiral $la\bar{3}d$ phase and no $I23^{[*]}$ or $Iso_1^{[*]}$ phase can be observed, whereas compounds with alkyloxy chains, acting as donor-substituents ($\sigma_m + \sigma_p = -0.22$ for OC_4H_9)^[51] form a sequence $la\bar{3}d_{(L)}-I23^{[*]}-la\bar{3}d_{(S)}$ upon chain elongation.^[9b,44,45,53] The number of molecules in the cross-section of the networks (n_{rafr} , see Tables 3 and S5) is 3.5–3.8 for the fluorinated compounds and 4.5–4.6 for the NO_2 and CN substituted compounds.

Here the question arises which kind the $la\bar{3}d$ phase – long pitch or short pitch – is actually formed by compounds **2/X**. The twist angles of $7.9-8.3^\circ$ for the fluorinated and $7.2-7.4^\circ$ for the CN/ NO_2 substituted compounds are intermediate between the values expected for the two cases ($<7^\circ$ for $la\bar{3}d_{(S)}$ and $>9^\circ$ for $la\bar{3}d_{(L)}$, respectively).^[31,44,45] As previously shown, the chiral $I23^{[*]}$ phase can be induced between different $la\bar{3}d$ phase types, whereas no such phase is induced between $la\bar{3}d$

phases belonging to the same type.^[44,45,54-56] As shown in Figure 6 a stripe of an $I23^{[*]}$ phase with chiral conglomerate texture is observed in the contact region between the Cub_{bi} phase of **1/14**,^[44] known to form the $la\bar{3}d_{(S)}$ type, and the $la\bar{3}d$ phases of the compounds **2/CN**, **2/OCF₃** and **2/F₃**. This means that the developing concentration gradient leads to the sequence $la\bar{3}d_{(L)}-I23^{[*]}-la\bar{3}d_{(S)}$ with increasing concentration of compounds **2/X**. Therefore, the $la\bar{3}d$ phases of all these polar substituted compounds **2/X** must be considered as long pitch (low twist) $la\bar{3}d_{(L)}$ -type phases.

No mirror symmetry broken $Iso_1^{[*]}$ phase can be found besides any of the $la\bar{3}d_{(L)}$ phases of the polar substituted compounds **2/X** (Table 3), though, as shown in Figure 7 for compounds **2/NO₂** and **2/OCF₃**, a broad feature occurs in the DSC traces in the temperature range of the isotropic liquid state. This indicates a transition to a percolated Iso_1 phase before the

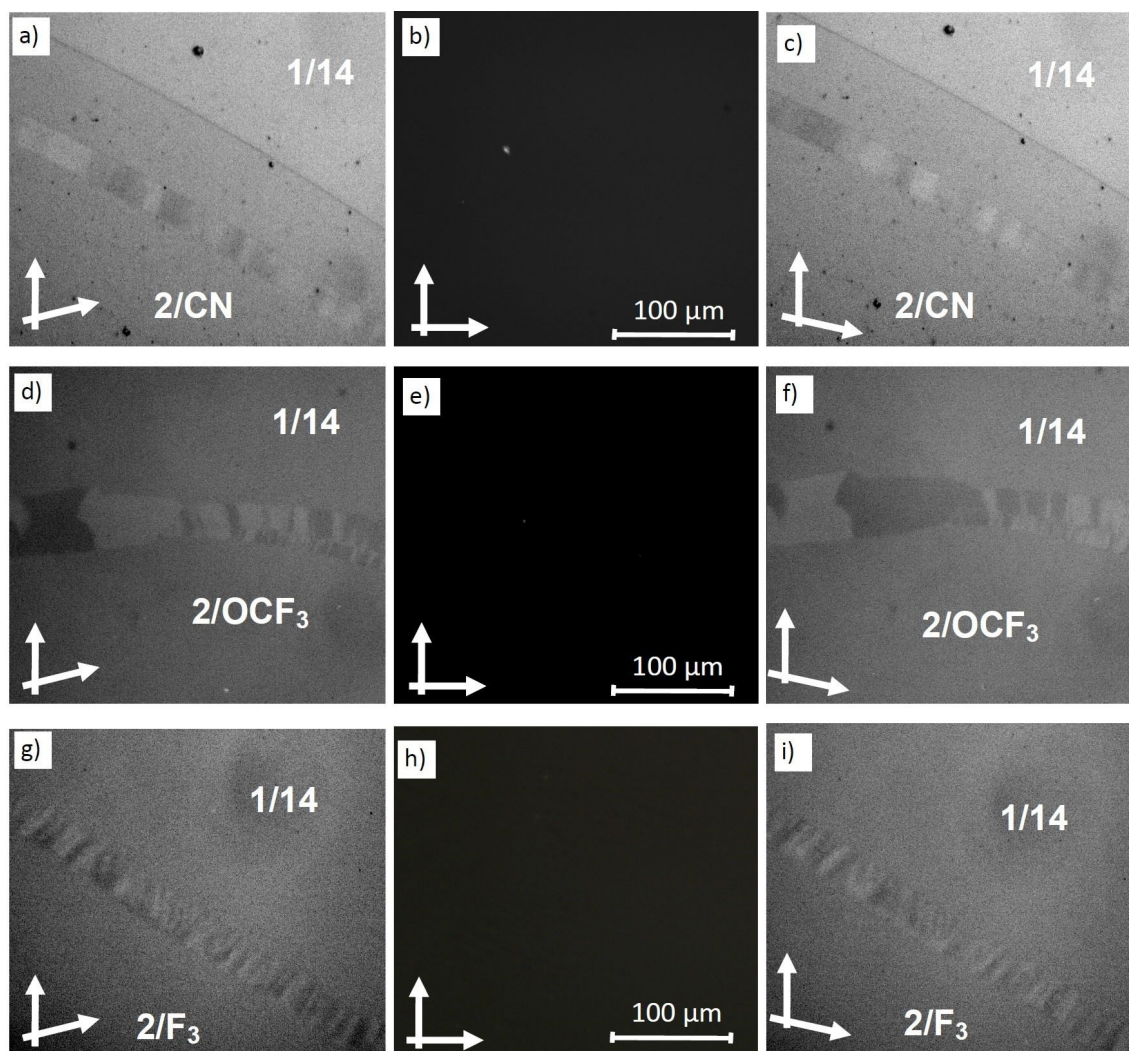


Figure 6. Development of chiral conglomerates of the induced $I23^{[*]}$ phase in the contact regions between the achiral $la\bar{3}d$ phases of a–c) **1/14** ($la\bar{3}d_{(S)}$)^[44] and **2/CN** at 149°C , d–f) **1/14** and **2/OCF₃** at 121°C and g–i) **1/14** with **2/F₃** at 126°C , at the left and right between slightly rotated polarizers and in the middle between crossed polarizers. The induction of a $I23^{[*]}$ ribbon indicates that both $la\bar{3}d$ phases should have different structure, that is, that they represent $la\bar{3}d_{(L)}$ phases for compounds **2/X**. The absence of any birefringence between crossed polarizers indicates the absence of any induced birefringent non-cubic mesophases and the inversion of the brightness by inverting the direction of the analyzer indicates the presence of a chiral conglomerate in the $I23^{[*]}$ ribbons; the phase boundary in a, c) represents the Iso_1-Cub_{bi} transition of the **1/14** + **2/CN** mixture.

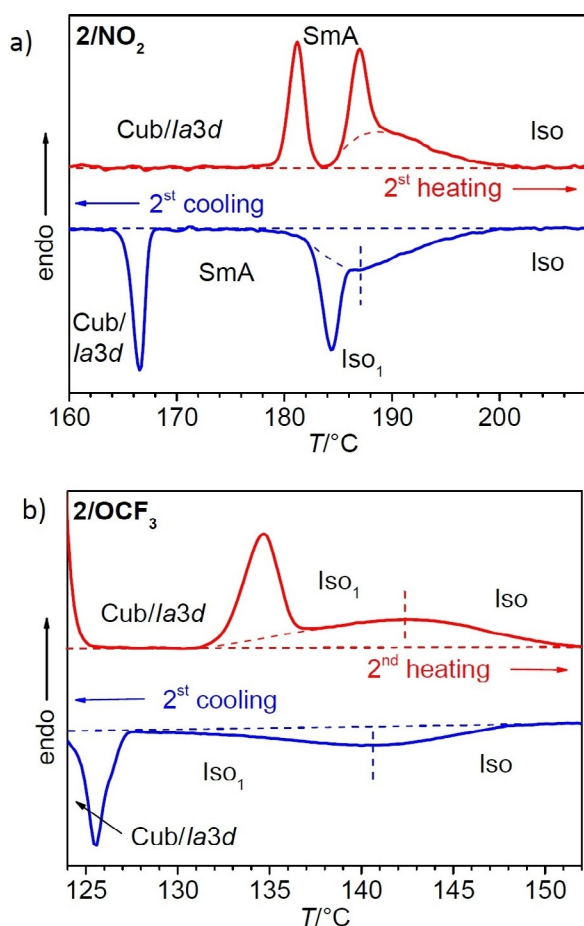


Figure 7. Representative DSC heating and cooling traces of compounds **2/X** showing a) the Iso–Iso₁–SmA–Cub_{bi}/*la*3d_(L) transition of **2/NO₂** and b) the Iso–Iso₁–Cub_{bi}/*la*3d_(L) transition of **2/OCF₃**; for full scans and the DSC traces of the other compounds, see Figure S1 d,g.

cubic phase is formed (see also Figure S1), independent if the *la*3d_(L) phase is separated from the isotropic liquid phase by an additional SmA range (**2/NO₂**, **2/CN**, Figure 7a and Figure S1 e) or not (**2/OCF₃**, **2/F_{nr}**, Figure 7b and Figure S1 h–j). This shape of the diffuse DSC feature is similar to that observed for compound **4/14** (Figure 3a) and the ANBCs.^[32b,c] In contrast, other polycatenar compounds, like the 5,5'-diphenyl-2,2'-dithiophene bisbenzoates (Scheme 1) do not show this kind of Iso–Iso₁ transition.^[29a,45] Related Iso–Iso₁ transitions were previously reported in the series of the hydrogen bonded dimers of the ANBCs with hydrogen bonding forming the rod-like cores, but not for the BABHs with *intermolecular* hydrogen bonding between the cores (see Scheme 1),^[9b,49a] providing stronger core–core interactions. The absence of an Iso–Iso₁ transition in some cases could therefore be interpreted by a network structure of the liquid phase, being present in the whole range of the isotropic liquid state. This would mean that the isotropic liquids of the strongly aggregating molecules can be considered as Iso₁ phases, being present in the whole investigated temperature range of the liquid state even at high temperatures, whereas for the weakly aggregating bent benzil derivatives they develop only shortly before the transition to the Cub_{bi} phase. Over-

all, the broad Iso–Iso₁ transition appears to occur adjacent to LC network phases if the network develops in a limited pre-transitional temperature range of the liquid phase.^[9b,38,49a]

Chirality synchronization by transition to the mirror symmetry broken Iso₁^[*] phase, takes place after reaching a certain degree of network connectivity, which is independent if there is an observable Iso–Iso₁ transition (Figure 8a,b,d) or not,^[45,47] meaning that chirality synchronization in the liquid state takes place after the dynamic network with a sufficient degree of connectivity has developed. However, not in all cases of liquid network phases (Iso₁) mirror symmetry breaking with formation of the Iso₁^[*] phase takes place (Figures 7 and 8c,d). The reason could either be an insufficient connectivity of the network achieved in the liquid state or a tendency to develop a racemic *la*3d-like network structure (see further below).

Non-symmetric tetracatenars with additional fluorine substitution at the less substituted terminal

Compound **1/6**^[44] was shown in previous work to form a unique sequence of three mirror symmetry broken phases with conglomerate texture (Figure 8a). At the transition from the ordinary isotropic liquid (Iso) on cooling a percolated Iso₁ phase is formed around 130 °C. This is achiral and becomes chiral at the next phase transition at 123 °C which is attributed to a transition to an Iso₁^[*] network phase. This turns into the chiral Cub_{bi}/*l*23^[*] phase at 118 °C which then on further cooling crystallizes at 61 °C with formation of an optically isotropic crystalline mesophase Cr_{iso}^[*] composed of a chiral conglomerate (Figure 8a and Table 4).^[44] Fluorination in the peripheral 3-position at the less substituted end (compound **3/2F6**) retains the fundamental phase sequence, though the Iso₁^[*] phase is only observable on cooling and the isotropic Cr_{iso}^[*] phase is replaced by a birefringent crystalline phase (Cr), see Table 4 and Figure S1 k,l.

Fluorination at the inside directed 2-position (**3/2F6**) retains the mirror symmetry broken Iso₁^[*] and Cr_{iso}^[*] phases, but removes the cubic *l*23^[*] phase of **1/6** completely, that is, there is a direct transition Iso₁^[*] to Cr_{iso}^[*] (Table 4, Figure 9 and Figure S1 m). There is no observable change of the conglomerate texture at the transition from Iso₁^[*] to Cr_{iso}^[*] (Figure 9a–d), though it is associated with a significant transition enthalpy of 22–24 kJ mol⁻¹.^[57] As also observed for **1/6**,^[44] the SAXS pattern of the Cr_{iso}^[*] phase of **3/2F6** is characterized by a relatively broad scattering, with a maximum at *d* = 5.35 nm, being very similar to the length of intercalated molecular pairs (Figure 9 f). The broadening of the small angle scattering indicates a distorted structure with short correlation length of ≈ 30 nm (Scherrer equation) corresponding to about 5–6 network distances. The multiple wide-angle scatterings indicate a crystalline phase (Figure 9g) and can be attributed to the mean alkyl chain distance (0.43 nm) and the lateral edge-to-edge and face-to-face packing of the aromatics (0.56/0.37 nm), very similar to the Cr_{iso}^[*] phase reported for **1/6**.^[44] The unusually low intensity of the wide angle scatterings (see Figure S6)^[58] and the optical isotropy are in line with a strongly distorted structure with crystallized polyaromatic cores and alkyl chain seg-

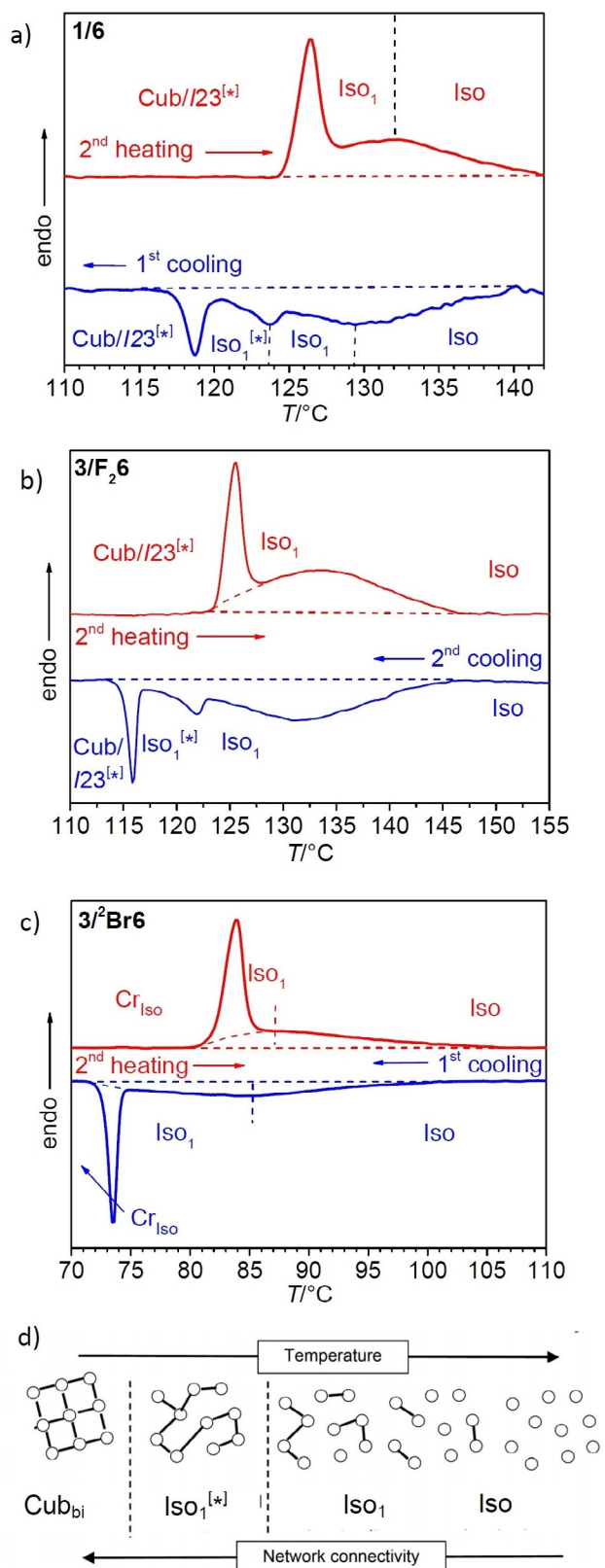


Figure 8. a–c) Representative DSC heating and cooling traces of a) compound 1/6 and b,c) the laterally core halogenated compounds 3/Y6;^[44] a,b) Iso–Iso₁–Iso₁^[*]–Cub_{bi}//I23^[*] transitions of compounds a) 1/6 and b) 3/F₂6 and c) Iso–Iso₁–Cr_{Iso} transition of compound 3/Br6; for full scans and the DSC traces of 3/F₂6 and 3/Br6, see Figure S1 o,q. d) Schematic sketch showing the transition from Iso via a cybotactic and a percolated liquid to Cub_{bi} by increasing transient network connectivity, the dots represent locally ordered clusters and the lines indicate the connections between them, the vertical dotted lines indicate phase transitions.

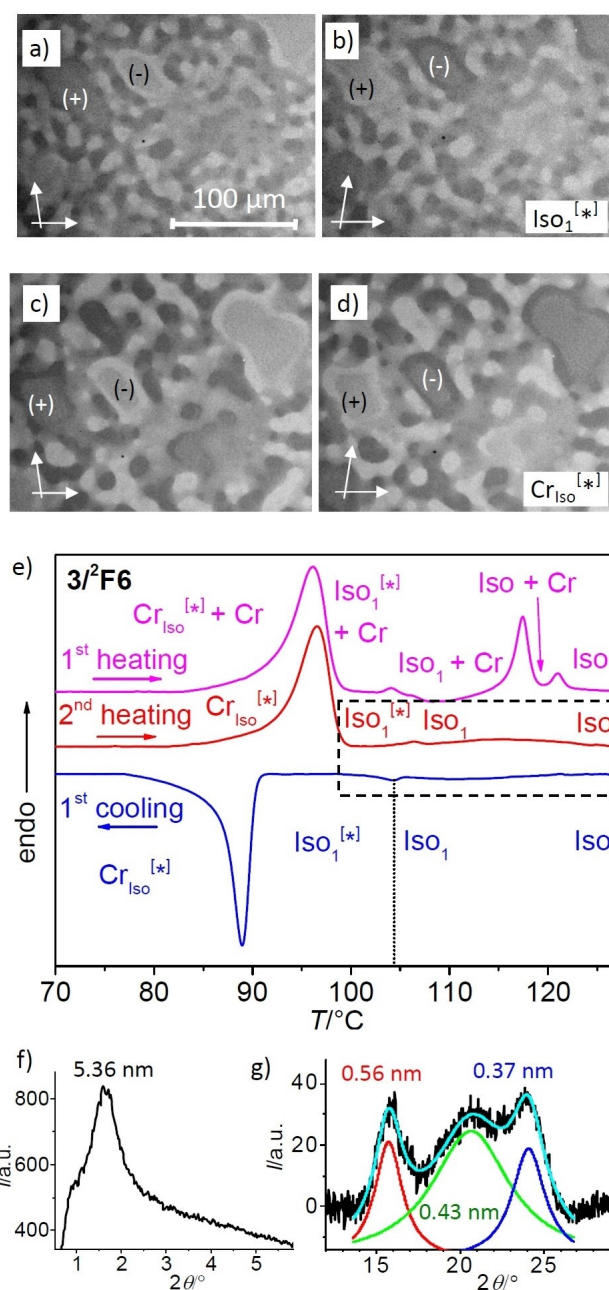


Figure 9. Investigation of compound 3/2F6. a,b) optically active domains in the Iso₁^[*] phase at 100°C and c,d) in the Cr_{Iso}^[*] phase at 60°C, as observed between slightly uncrossed polarizers after rotation in a), c) anticlockwise and b), d) clockwise direction (contrast enhanced). The different degrees of intermediate brightness result from overlapping with surface films having opposite chirality; e) shows the complete DSC heating and cooling traces (the section indicated by the dashed rectangle is shown in Figure S1 m); f) small angle and g) wide angle X-ray scattering pattern in the Cr_{Iso}^[*] phase at 25°C (see also Figure S5 for the complete pattern).

ments, with the disordered segments of the chains filling the remaining space.^[59,60] Additional birefringent crystalline phases with melting points at 117 and 121°C (magenta curve in Figure 9e) slowly crystallize from the Iso₁ or Iso phases, meaning that all mesophases of 3/2F6 are metastable.

Either chain elongation (3/2F10) or 2,3-difluorination (3/F26) recovers the I23^[*] phase and retains the Iso₁^[*] phase, whereas

Table 4. Comparison of the phase transitions of compounds **3/Yn** having additional lateral halogen substituents.^[a]

Compound	<i>n</i>	Y ³	Y ²	<i>T</i> [°C] [ΔH in kJ mol ⁻¹] ^[a]	<i>a</i> _{cub} [nm]
1/6 ^[44]	6	H	H	H: Cr 118 [64.6] (Cr _{Iso} ^[*] 82 [17.3]) I23 ^[*] 126 [2.2] Iso ₁ 134 [5.7] Iso C: Iso 130 [-7.1] Iso ₁ 123 [-0.5] Iso ₁ ^[*] 118 [-1.1] I23 ^[*] 61 [-15.3] Cr _{Iso} ^[*]	18.1
3/^βF6	6	F	H	H: Cr 93 [54.6] I23 ^[*] 116 [0.4] Iso ₁ 126 [9.5] Iso C: Iso 123 [-7.4] Iso ₁ 108 [-0.2] Iso ₁ ^[*] 103 [-0.8] I23 ^[*] 78 [-17.0] Cr	17.1
3/^βF6	6	H	F	H: Cr 121 ^[b] (Cr _{Iso} ^[*] 96 [24.5] Iso ₁ ^[*] 106 [0.2] Iso ₁ 114 [3.0]) Iso C: Iso 111 [-3.1] Iso ₁ 104 [-0.2] Iso ₁ ^[*] 89 [-21.5] Cr _{Iso} ^[*]	–
3/^βF10	10	H	F	H: Cr 103 [45.5] I23 ^[*] 113 [1.5] Iso ₁ 121 [4.3] Iso C: Iso 120 [-4.1] Iso ₁ 111 [-0.3] Iso ₁ ^[*] 101 [-0.5] I23 ^[*] 82 [-31] Cr	18.1
3/F₂6	6	F	F	H: Cr 93 [16.4] I23 ^[*] 126 [2.1] Iso ₁ 133 [2.4] Iso C: Iso 131 [-2.1] Iso ₁ 122 [-0.3] Iso ₁ ^[*] 117 [-0.9] I23 ^[*] 80 [17] Cr	17.2
3/^βCl6	6	H	Cl	H: Cr 109 [67.2] (Cr _{Iso} 84 [29.0] Iso ₁ 93 [3.0]) Iso C: Iso 86 [-2.1] Iso ₁ 78 [-0.2] <i>la</i> $\bar{3}$ <i>d</i> ₍₅₎ 73 [-22.3] Cr _{Iso}	–
3/^βBr6	6	H	Br	H: Cr 77 [21.0] (<i>la</i> $\bar{3}$ <i>d</i> ₍₅₎ ^[c] 80 ^[d]) Cr _{Iso} 84 [4.2] Iso ₁ 90 [3.4] Iso C: Iso 85 [-4.5] Iso ₁ 73 [-2.4] Cr _{Iso}	–

[a] DSC peak temperatures on heating/cooling (H/C) at 10 Kmin⁻¹; values in brackets give monotropic phase transitions observed in the second heating scan; abbreviations: Cr = birefringent crystalline phase; Cr_{Iso} = optically isotropic crystalline solid, Cr_{Iso}^[*] = mirror symmetry broken Cr_{Iso} phase; for the other abbreviations, see Table 1 and 3; phases shown in bold and with ^[*] indicate mirror symmetry broken phases; for DSCs, see Figures 8, 9 e and Figure S1; the maxima of the Iso–Iso₁ transitions are given, the corresponding temperature ranges are shown in Table S1. [b] Several crystalline modifications and crystallization processes take place in first heating, only the crystalline phase with highest melting point is given. [c] Due to crystallization no X-ray scattering could be performed. [d] The cubic phase can only be observed in the first heating as long as Cr_{Iso} is not formed.

the Cr_{Iso}^[*] phase is removed and replaced by a birefringent crystalline phase (Table 4). Note that the Cub_{bi}–Iso₁ transition temperature of the difluorinated compound **3/F₂6** (Figure 8c, Figure S1 o) is almost the same as that observed for the non-fluorinated compound **1/6**, meaning that the steric mesophase destabilizing effect of 2-substitution is compensated by the additional electron attracting substituent in 3-position, strengthening the intermolecular attraction.

Investigation of the development of the correlation length ζ of the clusters in the isotropic phase range by SAXS on cooling was conducted for compound **3/F₂6** as example. The $\zeta = f(T)$ curve is characterized by an increase of the slope at around 145–150 °C (Figure 10). This coincides with the onset of the broad DSC feature of the Iso–Iso₁ transition (Figure 8a). The correlation length increases continuously from 13 nm to 36 nm in the Iso₁^[*] phase without any distinct jump at the phase transitions. This is in line with the proposed model of the Iso–Iso₁^[*] transition. The increase of the *d*-value of the small angle scattering is also continuous, which is mainly attributed to the transition from a diffuse scattering, not following the Bragg law, to a more Bragg-like character of this scattering upon approaching the Cub_{bi} phase. Similar observations were made for **3/^βF6**, see Figure S5.

Non-symmetric tetracatenars with other halogens at the less substituted terminal

The effect of replacing fluorine by the larger halogens Cl or Br was investigated for the series **3/^βY6** with the halogen in the

2-position (compounds **3/^βCl6** and **3/^βBr6**, see Table 4). The reason for choosing this position is that changes in this position provide a stronger effect on the self-assembly than in the 3-position. For example, for **3/^βF6** the fundamental phase sequence of **3/6** is retained, whereas the chiral **I23**^[*] phase is removed for **3/^βF6**. Interestingly, replacing the fluorine of **3/^βF6** by chlorine restores the Cub_{bi} phase, but the space group is changed to the achiral *la* $\bar{3}$ *d* phase, which occurs adjacent to the achiral Iso₁ phase without additional Iso₁^[*] range. More-

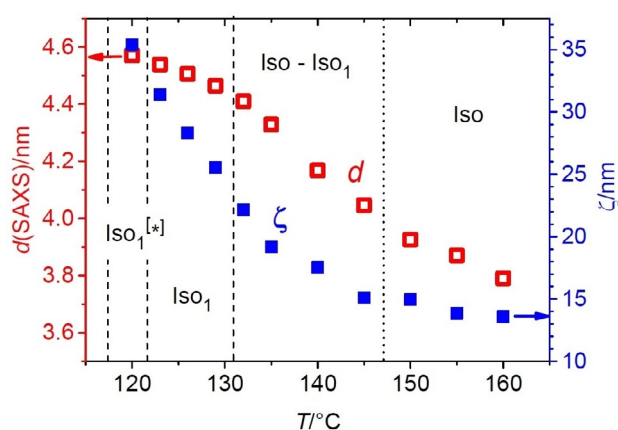


Figure 10. Temperature dependence of the *d*-value of the small angle scattering and the correlation length (calculated with the Scherrer equation) of the clusters in the Iso phases of compound **3/F₂6**, measured on cooling; for the DSC traces see Figure 8b; the lift-off temperature of the broad DSC feature on cooling is around 147 °C, see Figure S5 for the related curve of **3/^βF6**.

over, the $la\bar{3}d$ phases of $3/2\text{Cl6}$ and $3/2\text{Br6}$ are only monotropic and appear in small temperature ranges, observable only on heating (Table 4).^[61] Though, due to partial crystallization, these Cub_{bi} phases are not accessible to X-ray scattering experiments, they can be investigated by POM. As shown in Figure S2d–f, in the contact region between the (previously confirmed) $\text{Cub}_{\text{bi}}/la\bar{3}d_{(\text{S})}$ phase of $1/14$ ^[44] and the $la\bar{3}d$ phase of compound $3/2\text{Br6}$ no $I23^{[*]}$ phase with chiral conglomerate texture is observed, meaning that this Cub_{bi} phase is of the same short pitch $la\bar{3}d_{(\text{S})}$ type. The increasing size of the lateral 2-substituent in the order $\text{H} < \text{F} < \text{Cl} < \text{Br}$ obviously changes the cubic space group from $I23^{[*]}$ to $la\bar{3}d_{(\text{S})}$, similar to the effect of alkyl chain elongation in the series $1/n$. The crystalline mesophase formed upon further cooling is also optically isotropic as that formed by the fluorinated compound $3/2\text{F6}$, but in this case it is achiral (Cr_{iso}). It is likely that the network structure in this crystalline mesophase is $la\bar{3}d$ -like, as in the adjacent cubic phase, which is intrinsically achiral (racemic). Also the chirality synchronization in the liquid state is affected by the size of the halogen. Whereas for the non-fluorinated compound $1/6$ and all three investigated fluorinated compounds $3/2\text{F6}$, $3/2\text{Br6}$ and $3/2\text{Cl6}$ chirality synchronization takes place in the temperature range of the percolated liquid phase ($\text{Iso}_1^{[*]}$, see Figure 8b,c) it is not observed for $3/2\text{Cl6}$ and $3/2\text{Br6}$. A possible reason could be that the local network structure in the percolated Iso_1 phase also becomes $la\bar{3}d$ -like by the steric effect of these larger halogens and therefore is intrinsically achiral.

Local versus total mirror symmetry breaking

It is noted that the observed conglomerate formation represents only a local mode of mirror symmetry breaking. Total mirror symmetry breaking with stochastic outcome on a macroscopic length scale can be achieved in the $I23^{[*]}$ phase if seed formation is slow and growth of the cubic phase is fast and it becomes deterministic in the presence of traces of external sources of chirality.^[8,29a,38,47a] Related effects were also observed in the mirror symmetry broken soft crystalline phases formed by mesogenic trimers.^[62] Tiny chirality sources are also assumed to be responsible for “spontaneous” formation of $I23^{[*]}$ or $\text{Iso}_1^{[*]}$ phases with uniform chirality, as observed in some cases.^[8] However, for the benzil-based compounds the tendency to form large homogeneous chiral domains is less developed if compared with related 2,2'-bithiophene based polycatenars^[29a,46] and formation of relatively small chiral domains is dominating in this class of compounds (see Figures 2a–c and 9a–d). A possible reason could be a higher viscosity or the bent molecular shape, slowing down the growth processes.

Discussion of the importance of network formation for chirality synchronization

Chirality synchronization of the local helical structure by network formation, suppressing helix reversal defects,^[63] appears to be the key feature required for mirror symmetry breaking of polycatenar mesogens in the liquid, LC and soft crystalline

states. The helical networks, developing in the $\text{Iso}_1/\text{Iso}_1^{[*]}$ and $\text{Cub}_{\text{bi}}/la\bar{3}d/I23^{[*]}$ phases, can obviously be retained after crystallization of the aromatic cores in the optically isotropic crystalline mesophases of compounds $3/2\text{Yn}$, where the polyaromatic cores and parts of the alkyl chains assume a crystalline packing in the networks and the disordered segments of the alkyl chains fill the remaining space. These crystalline mesophases are in some respect related to gels (“solvent free gels”),^[43,59,60,62,64–66] though details of their structures require further investigations. A certain degree of net connectivity is in some cases also retained in the isotropic liquid phases, considered as percolated liquids^[67,68] and representing dynamic networks, which become chiral after crossing the critical network density required for emergence of chirality synchronization.^[47,38] These percolated liquids can either transform into chirality synchronized cubic LC phases after assuming long-range periodicity or to disordered crystalline isotropic mesophases by freezing the molecular mobility.

For numerous compounds local clusters and network formation occur in the liquid state prior to the transition to LC and crystalline phases. Often, these transitions take place already at high temperatures outside the investigated (or accessible) temperature range, or do not show up in the DSC traces, because they take place over extremely broad temperature ranges. However, the DSC features of the Iso - Iso_1 transitions of the benzil-derived polycatenars appear in relatively narrow temperature ranges close to the phase transition to the Cub_{bi} phase and, therefore, become easily detectable. Similar observations were made for the ANBCs (Scheme 1).^[9b,29a,32b,c,49a] This kind of polyamorphism in the liquid state appears to be associated with network formation and therefore is observed in the vicinity of Cub_{bi} phases. It can also be found if a lamellar or columnar phase separates the Iso_1 and Cub_{bi} phase (compounds $2/\text{CN}$ and $2/\text{NO}_2$, Figure 7a). It is however not observed at the transition to non-cubic LC phases, which are (with respect to molecular structure or temperature) far away from any Cub_{bi} phase range. Moreover, it appears to require a certain strength of the attractive intermolecular interactions, being strong enough for network formation and sufficiently weak that the networks can be disrupted by mild thermal agitation. Depending on the kind of network structure, the resulting liquid, LC or crystalline mesophases can be optically inactive if a racemic double network ($la\bar{3}d$) is formed, or optically active if a homochiral triple network develops ($I23^{[*]}$). As the local structure can change at the phase transitions also phase sequences combining chiral and achiral phases can occasionally be observed (e.g. $la\bar{3}d$ - $\text{Iso}_1^{[*]}$).

An important point concerns the formation of the $I23^{[*]}$ structure instead of the usually dominating double gyroid ($la\bar{3}d$) structure, which is only observed if rod-like units are involved in the molecules, leading to a helical twist along the networks.^[29] Therefore, it can be assumed that this transition is chirality (helicity) induced. One way of thinking considers the matching of the twist at the nodes in the individual nets (intra-network resonance) as important for chirality synchronization.^[29a] A second important issue concerns the through-space interaction between the nets, that is, the interaction between

adjacent close packed helix segments. Here a slight change of the twist angle of the molecules along the helices could modify the sign and strength of inter-helix interactions at a given angle and distance between the close packed adjacent helices.^[69] Preferred heterochiral interactions are obviously compatible with the $la\bar{3}d$ phase structure composed of two enantiomeric networks, leading to chiral extinction (lowest energy racemic state). However, an increasing preference of homochiral helix-helix interaction (lowest energy homochiral state) could destabilize the double gyroid structure and requires a change of the phase structure by retaining the network topology involving exclusively three way junctions. The $I23^{[*]}$ structure appears to be the best solution for this case, though also non-cubic arrangements of helical networks, as for example in the tetragonal "SmQ phase",^[40] could have very similar energy and can compete under certain conditions.

The softening of the helix-helix interactions in the liquid state could change the preferred mode of helix correlation and this could explain the transition between an achiral double gyroid cubic phase and a conglomerate type $Iso_1^{[*]}$ liquid (with assumed local $I23$ structure) observed in some cases. Though there is a substantial amount of work concerning the investigation of helix-helix interactions in lipid membranes,^[70] the general understanding of the helix packing depending on the sign and strength of the interaction parameters, the helical twist, and the angle between the interacting helices needs to be studied and simulated in more detail to support this hypothesis.^[69]

It is noted that there is a strong relation between the Cub_{bi} - $Iso^{[*]}$ transitions reported here for achiral molecules (with transiently chiral conformations) and the BPI/BPII to BPIII (BP = blue phase) transition observed for permanently chiral rod-like molecules.^[71,72] The cubic BPII, for example, has a $la\bar{3}d$ double gyroid structure, whereas the BPIII (blue fog phase) is an isotropic liquid with dynamic network structure.^[71a] Even the typical DSC features of the BPI/BPII to BPIII transitions resemble those of the Cub_{bi} - $Iso^{[*]}$ transitions, characterized by a broad diffuse feature in the liquid state.^[49a] The main difference is that in the case of the Blue Phases the network structure is induced by a permanent molecular chirality, whereas for the achiral polycatenar compounds reported here the network structure leads to chirality synchronization, destabilizing the achiral/racemic states which then spontaneously bifurcate into a conglomerate of chiral liquids due to the emergent cooperativity of chirality transfer provided by the network structure.^[8]

Conclusions

It is shown that the 4,4'-diphenylbenzil unit is a universal transiently chiral bent building block for the design of mesogens capable of forming network structures in the liquid, the LC and the crystalline state. Cub_{bi} network structures with $la\bar{3}d$ and $I23^{[*]}$ space groups were obtained for non-symmetric tetracatenars (compounds **1/n**, **4/n** and **3/Yn**) and tricaténars (compounds **2/X**) if the total number of benzene rings incorporated in the core unit is at least five. Polar substituents at the apex (X) were shown to support cubic phase formation, leading to

compounds with high transition temperatures and wide cubic ranges. These polar substituents represent strong electron acceptors which reduce the electron density of the π -system of the cores and this strengthens the attractive core-core interactions, thus stabilizing the cubic phases significantly, even against unfavorable steric effects of these substituents (Table 3). The mesophase stabilizing effect grows in the order $X = F < OCF_3 < CN < NO_2$, roughly corresponding to the increasing Hammett constants of these substituents (Figure 11).^[51] The cubic phases of all these compounds with a relatively small polar apex represent long pitch $la\bar{3}d_{(L)}$ phases, thus indicating a small helical twist between the molecules along the networks. Larger twist angles, supporting the formation of the mirror symmetry broken $I23^{[*]}$ phase, were achieved for compounds with longer alkoxy chains at the apex. Halogenation of the monoalkoxylated benzene ring of these tetracatenars further supports the helical twist, leading to a transition from $I23^{[*]}$ to the achiral short pitch $la\bar{3}d_{(S)}$ phase for the larger halogens Cl and Br (Figure 11). Especially strong is this effect in the inside directed 2-position. Besides the effect on the twist, there is also a steric mesophase destabilizing effect of the polar substituents X and Y, becoming more important in the sequence of their positions $4 < 3 < 2$. Thus, the steric effects of the substituents can override the stabilizing electronic effects, the more they are shifted towards the center of the polyaromatic core.^[73,74] Figure 11 summarizes the relations between molecular structure and formation of the distinct cubic and accompanying mirror symmetry broken $Iso_1^{[*]}$ phases gained herein.

Overall, this work contributes to the better understanding of the development of networks and spontaneous mirror symmetry breaking in self-assembled systems, including crystalline helical aggregates,^[43,64-75] gels,^[60,66] LC phases^[38,59,60,62,76-79] and

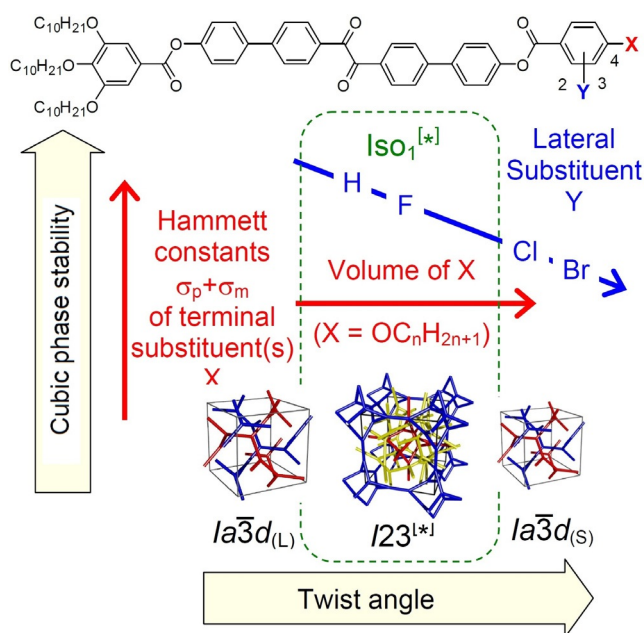


Figure 11. Summary of the relations between molecular structure, cubic phase type, cubic phase stability and mirror symmetry breaking in the LC and isotropic liquid phases.

the most intriguing case of mirror-symmetry broken isotropic liquids.^[47] In general, the nano-structures of the liquid phases and their polyamorphism (liquid–liquid phase transitions and liquid–liquid phase separations) are still less investigated and represent almost unsolved scientific problems with great importance.^[80] It appears that formation of cybotactic clusters and dynamic networks are important features with relevance for the understanding of the special properties of fluids, especially in the context of prebiotic and biological systems.^[8] Dynamic network formation in liquids is a prerequisite for development of complexity and obviously provides the basis of the emergence of new features. Among them the bifurcation of achiral and racemic systems into stable homochiral states, thus leading to the transition from achiral to chiral chemical systems, representing the first step of the transition from chemical systems to biogenesis.^[8]

Acknowledgements

This Work was supported by the Deutsche Forschungsgemeinschaft (Ts 39/24-2). Open access funding enabled and organized by Projekt DEAL.

Conflict of interest

The authors declare no conflict of interest.

Keywords: chirality · cubic phases · liquid crystals · mirror symmetry breaking · soft matter

- [1] J. Gasteiger, J. Zupan, *Angew. Chem. Int. Ed. Engl.* **1993**, *32*, 503–527; *Angew. Chem.* **1993**, *105*, 510–536.
- [2] S. Kauffman, *At Home in the Universe*, Oxford University Press, Oxford, **1995**, pp. 54–58.
- [3] a) A. S. Y. Wong, W. T. S. Huck, *Beilstein J. Org. Chem.* **2017**, *13*, 1486–1497; b) S. Otto, *Acc. Chem. Res.* **2012**, *45*, 2200–2210; c) B. A. Grzybowski, K. Fitzner, J. Paczesny, S. Granick, *Chem. Soc. Rev.* **2017**, *46*, 5647–5678.
- [4] M. O’Keeffe, O. M. Yaghi, *Chem. Rev.* **2012**, *112*, 675–702.
- [5] T. Kato, J. Uchida, T. Ichikawa, T. Sakamoto, *Angew. Chem. Int. Ed.* **2018**, *57*, 4355–4371; *Angew. Chem.* **2018**, *130*, 4438–4455.
- [6] *Bicontinuous Liquid Crystals* (Eds.: M. L. Lynch, P. T. Spicer), CRC Press, Boca Raton, **2005**.
- [7] A. Guijarro, M. Yus, *The Origin of Chirality in the Molecules of Life*, Royal Society of Chemistry, Cambridge, **2009**.
- [8] C. Tschierske, C. Dressel, *Symmetry* **2020**, *12*, 1098.
- [9] a) G. Ungar, F. Liu, X. B. Zeng in *Handbook of Liquid Crystals, Vol 5* 2nd ed. (Eds.: J. W. Goodby, P. J. Collings, T. Kato, C. Tschierske, H. Gleeson, P. Raynes), Wiley-VCH, Weinheim, **2014**; b) S. Kutsumizu, *Isr. J. Chem.* **2012**, *52*, 844–853.
- [10] C. Tschierske, *Angew. Chem. Int. Ed.* **2013**, *52*, 8828–8878; *Angew. Chem.* **2013**, *125*, 8992–9047.
- [11] K. Borisch, S. Diele, P. Göring, H. Kresse, C. Tschierske, *J. Mater. Chem.* **1998**, *8*, 529–543.
- [12] a) A. J. Meuler, M. A. Hillmyer, F. S. Bates, *Macromolecules* **2009**, *42*, 7221–7250; b) E. L. Thomas, *Sci. China Chem.* **2018**, *61*, 25–32.
- [13] a) J. M. Seddon, R. H. Templer in *Handbook of Biological Physics, Vol. 1* (Eds.: R. Lipowsky, E. Sackmann), Elsevier, Amsterdam, **1995**, pp. 97–160; b) S. T. Hyde in *Handbook of Applied Surface and Colloid Chemistry, Vol 1* (Ed. K. Holmberg), Wiley, New York, **2001**, pp. 299–332; c) L. van ’t Hag, S. L. Gras, C. E. Conn, C. J. Drummond, *Chem. Soc. Rev.* **2017**, *46*, 2705–2731.
- [14] L. Han, S. Che, *Adv. Mater.* **2018**, *30*, 1705708.
- [15] a) C. Tschierske, *J. Mater. Chem.* **2001**, *11*, 2647–2671; b) C. Tschierske, *Annu. Rep. Prog. Chem. Sect. C* **2001**, *97*, 191–267; c) C. Tschierske, *Isr. J. Chem.* **2012**, *52*, 935–959; d) C. Tschierske in *Handbook of Liquid Crystals, Vol. 5*, 2nd ed. (Eds.: J. W. Goodby, J. P. Collings, T. Kato, C. Tschierske, H. F. Gleeson, P. Raynes), Wiley-VCH, Weinheim, **2014**, pp. 1–88.
- [16] a) J.-H. Ryu, M. Lee, *Struct. Bonding (Berlin)* **2008**, *128*, 63–98; b) L.-Y. Shi, Y. Zhou, X.-H. Fan, Z. Shen, *Macromolecules* **2013**, *46*, 5308–5316.
- [17] X. Zeng, M. Prehm, G. Ungar, C. Tschierske, F. Liu, *Angew. Chem. Int. Ed.* **2016**, *55*, 8324–8327; *Angew. Chem.* **2016**, *128*, 8464–8467.
- [18] X. Zeng, S. Poppe, A. Lehmann, M. Prehm, C. Chen, F. Liu, H. Lu, G. Ungar, C. Tschierske, *Angew. Chem. Int. Ed.* **2019**, *58*, 7375–7379; *Angew. Chem.* **2019**, *131*, 7453–7457.
- [19] S. Poppe, X. Cheng, C. Chen, X. Zeng, R.-B. Zhang, F. Liu, G. Ungar, C. Tschierske, *J. Am. Chem. Soc.* **2020**, *142*, 3296–3300.
- [20] C. Chen, R. Kieffer, H. Ebert, M. Prehm, R.-B. Zhang, X. Zeng, F. Liu, G. Ungar, C. Tschierske, *Angew. Chem. Int. Ed.* **2020**, *59*, 2725–2729; *Angew. Chem.* **2020**, *132*, 2747–2751.
- [21] a) F. Liu, M. Prehm, X. Zeng, C. Tschierske, G. Ungar, *J. Am. Chem. Soc.* **2014**, *136*, 6846–6849; b) S. Poppe, C. Chen, F. Liu, C. Tschierske, *Chem. Commun.* **2018**, *54*, 11196–11199.
- [22] A. M. Levelut, M. Clerc, *Liqu. Cryst.* **1998**, *24*, 105–115.
- [23] X. B. Zeng, G. Ungar, M. Imperor-Clerc, *Nat. Mater.* **2005**, *4*, 562–567.
- [24] X.-Q. Jiang, R.-Y. Zhao, W.-Y. Chang, D.-X. Yin, Y.-C. Guo, W. Wang, D.-H. Liang, S. Yang, A.-C. Shi, E.-Q. Chen, *Macromolecules* **2019**, *52*, 5033–5041.
- [25] Y. Sun, P. Padmanabhan, M. Misra, F. A. Escobedo, *Soft Matter* **2017**, *13*, 8542–8555.
- [26] There are only few reports about bicontinuous networks having the aromatic core on the minimal surface, either parallel^[20] or perpendicular to them.^[27]
- [27] M. Poppe, C. Chen, F. Liu, S. Poppe, C. Tschierske, *Chem. Eur. J.* **2017**, *23*, 7196–7200.
- [28] S. Andersson, S. T. Hyde, K. Larsson, S. Lidin, *Chem. Rev.* **1988**, *88*, 221–242.
- [29] a) C. Dressel, F. Liu, M. Prehm, X. B. Zeng, G. Ungar, C. Tschierske, *Angew. Chem. Int. Ed.* **2014**, *53*, 13115–13120; *Angew. Chem.* **2014**, *126*, 13331–13336; b) M. Alaasar, S. Poppe, Q. Dong, F. Liu, C. Tschierske, *Chem. Commun.* **2016**, *52*, 13869–13872; c) Y. Cao, M. Alaasar, A. Nallapaneni, M. Salamończyk, P. Marinko, E. Gorecka, C. Tschierske, F. Liu, N. Vaupotič, C. Zhu, *Phys. Rev. Lett.* **2020**, *125*, 027801.
- [30] a) T. Kajitani, S. Kohmoto, M. Yamamoto, K. Kishikawa, *Chem. Mater.* **2005**, *17*, 3812–3819; b) J. M. Wolska, J. Wilk, D. Pocięcha, J. Mieczkowski, E. Gorecka, *Chem. Eur. J.* **2017**, *23*, 6853–6857; c) H. R. Brand, H. Pleiner, *Eur. Phys. J. E* **2019**, *42*, 142.
- [31] X. B. Zeng, G. Ungar, *J. Mater. Chem. C* **2020**, *8*, 5389–5398.
- [32] a) G. W. Gray, B. Jones, F. Marson, *J. Chem. Soc.* **1957**, 393–401; b) S. Kutsumizu, K. Morita, T. Ichikawa, S. Yano, S. Nojima, T. Yamaguchi, *Liq. Cryst.* **2002**, *29*, 1447–1458; c) S. Kutsumizu, M. Yamada, S. Yano, *Liq. Cryst.* **1994**, *16*, 1109–1113.
- [33] a) H. Schubert, J. Hauschild, D. Demus, S. Hoffmann, *Z. Chem.* **1978**, *18*, 256; b) Y. Yamamura, Y. Nakazawa, S. Kutsumizu, K. Saito, *Phys. Chem. Chem. Phys.* **2019**, *21*, 23705–23712.
- [34] S. Kutsumizu, I. Tokiwa, A. Kawafuchi, Y. Miwa, Y. Yamamura, K. Saito, *Phys. Chem. Chem. Phys.* **2016**, *18*, 9013–9020.
- [35] a) H. T. Nguyen, C. Destrade, J. Malthete, *Adv. Mater.* **1997**, *9*, 375–388; b) D. W. Bruce, *Acc. Chem. Res.* **2000**, *33*, 831–840; c) W. Weissflog in *Handbook of Liquid Crystals, Vol. 5* 2nd Ed. (Eds.: J. W. Goodby, J. P. Collings, T. Kato, C. Tschierske, H. F. Gleeson, P. Raynes), Wiley-VCH, Weinheim, **2014**, pp. 89–174.
- [36] In a similar way also silyl groups and perfluorinated alkyl chains could lead to Cub_{b1} phases due to the interface curvature provided by these bulky chains.^[15,34,37]
- [37] a) I. Nishiyama, *Chem. Rec.* **2009**, *9*, 340–355; b) M. Yoneya, *Chem. Rec.* **2011**, *11*, 66–76; c) E. Nishikawa, J. Yamamoto, H. Yokoyama, *J. Mater. Chem.* **2003**, *13*, 1887–1893; d) E. Nishikawa, E. T. Samulski, *Liq. Cryst.* **2000**, *27*, 1463–1471.
- [38] a) C. Tschierske, *Liqu. Cryst.* **2018**, *45*, 2221–2252; b) C. Tschierske, G. Ungar, *ChemPhysChem* **2016**, *17*, 9–26.
- [39] A. H. Schoen, *Interface Focus* **2012**, *2*, 658–668.

- [40] A similar synchronization of the network chirality was found in the non-cubic SmQ phase with 90° four-way junctions, see ref. [41].
- [41] H. J. Lu, X. B. Zeng, G. Ungar, C. Dressel, C. Tschierske, *Angew. Chem. Int. Ed.* **2018**, *57*, 2835–2840; *Angew. Chem.* **2018**, *130*, 2885–2890.
- [42] The effect of the alkyl chains in the LC phases is similar to the contribution of steric effects on helix formation in the case of the crystalline self-assembly in supramolecular polymers, leading to fibres and gels, see ref. [43].
- [43] Y. Dorca, E. E. Greciano, J. S. Valera, R. Gjmez, L. Sanchez, *Chem. Eur. J.* **2019**, *25*, 5848–5864; E. Yashima, N. Ousaka, D. Taura, K. Shimomura, T. Ikai, K. Maeda, *Chem. Rev.* **2016**, *116*, 13752–13990.
- [44] T. Reppe, S. Poppe, X. Cai, F. Liu, C. Tschierske, *Chem. Sci.* **2020**, *11*, 5902–5908.
- [45] T. Reppe, C. Dressel, S. Poppe, C. Tschierske, *Chem. Commun.* **2020**, *56*, 711–713.
- [46] C. Dressel, T. Reppe, S. Poppe, M. Prehm, H. Lu, X. Zeng, G. Ungar, C. Tschierske, *Adv. Funct. Mater.* **2020**, 2004353.
- [47] a) C. Dressel, T. Reppe, M. Prehm, M. Brautzsch, C. Tschierske, *Nat. Chem.* **2014**, *6*, 971–977; b) C. Dressel, W. Weissflog, C. Tschierske, *Chem. Commun.* **2015**, *51*, 15850–15853; c) M. Alaasar, M. Prehm, Y. Cao, F. Liu, C. Tschierske, *Angew. Chem. Int. Ed.* **2016**, *55*, 312–316; *Angew. Chem.* **2016**, *128*, 320–324; d) M. Alaasar, S. Poppe, Q. Dong, F. Liu, C. Tschierske, *Angew. Chem. Int. Ed.* **2017**, *56*, 10801–10805; *Angew. Chem.* **2017**, *129*, 10941–10945.
- [48] a) C. J. Brown, R. Sadanaga, *Acta Crystallogr.* **1965**, *18*, 158–164; b) Q. Shen, K. Hagen, *J. Phys. Chem.* **1987**, *91*, 1357–1360; c) Z. Pawelka, A. Koll, T. Zeegers-Huyskens, *J. Mol. Struct.* **2001**, *597*, 57–66.
- [49] a) J. W. Goodby, D. A. Dunmur, P. J. Collings, *Liq. Cryst.* **1995**, *19*, 703–709; b) A. Gradisek, M. Cifelli, M. Wojcik, T. Apih, S. V. Dvinskikh, E. Gorecka, V. Domenici, *Crystals* **2019**, *9*, 178.
- [50] J. W. Steed, J. L. Atwood, *Supramolecular Chemistry*, Wiley, Chichester, **2000**.
- [51] C. Hansch, A. Leo, R. W. Taft, *Chem. Rev.* **1991**, *91*, 165–195.
- [52] a) K. Kishikawa, *Isr. J. Chem.* **2012**, *52*, 800–808; b) M. Hird, *Chem. Soc. Rev.* **2007**, *36*, 2070–2095.
- [53] S. Kutsumizu, Y. Yamada, T. Sugimoto, N. Yamada, T. Udagawa, Y. Miwa, *Phys. Chem. Chem. Phys.* **2018**, *20*, 7953–7961.
- [54] S. Kutsumizu, S. Miisako, Y. Miwa, M. Kitagawa, Y. Yamamura, K. Saito, *Phys. Chem. Chem. Phys.* **2016**, *18*, 17341–17344.
- [55] As another case of chirality induction by mixing two components, the induction of a chiral N₁₈ phase was observed by mixing two achiral complementary hydrogen bonding molecules, see ref. [56].
- [56] R. Walker, D. Pocięcha, J. P. Abberley, A. Martinez-Felipe, D. A. Paterson, E. Forsyth, G. B. Lawrence, P. A. Henderson, J. M. D. Storey, E. Gorecka, C. T. Imrie, *Chem. Commun.* **2018**, *54*, 3383–3386.
- [57] Values on heating were used, because the values on cooling tend to be lower due to the slow transitions, which are partly suppressed in the cooling cycle.
- [58] R. Androsch, A. M. Rhoades, I. Stolte, C. Schick, *Eur. Polym. J.* **2015**, *66*, 180–189.
- [59] M. Alaasar, M. Prehm, C. Tschierske, *Chem. Commun.* **2013**, *49*, 11062–11064; M. Alaasar, M. Prehm, M. Brautzsch, C. Tschierske, *J. Mater. Chem. C* **2014**, *2*, 5487–5501; M. Alaasar, M. Prehm, M. Brautzsch, C. Tschierske, *Soft Matter* **2014**, *10*, 7285–7296; M. Alaasar, M. Prehm, C. Tschierske, *Chem. Eur. J.* **2016**, *22*, 6583–6597.
- [60] a) T. Otani, F. Araoka, K. Ishikawa, H. Takezoe, *J. Am. Chem. Soc.* **2009**, *131*, 12368–12372; b) A. Zep, M. Salamonczyk, N. Vaupotic, D. Pocięcha, E. Gorecka, *Chem. Commun.* **2013**, *49*, 3119–3121; c) S. Shadpour, A. Nemati, N. J. Boyd, L. Li, M. E. Prevot, S. L. Wakerlin, J. P. Vanegas, M. Salamonczyk, E. Hegmann, C. Zhu, M. R. Wilson, A. I. Jakli, T. Hegmann, *Mater. Horiz.* **2019**, *6*, 959–968.
- [61] The cubic phase is not observed on cooling due to the delay of the Iso₁-Cub_{bi} transition on cooling, so that only the Cr_{iso} phase can be found.
- [62] A. Yoshizawa, Y. Kato, H. Sasaki, Y. Takanishi, J. Yamamoto, *J. Phys. Chem. B* **2016**, *120*, 4843–4851; R. Oikawa, H. Sasaki, Y. Takanishi, M. Sagisaka, J. Yamamoto, A. Yoshizawa, *Soft Matter* **2019**, *15*, 3179–3187; M. Kurata, A. Yoshizawa, *Chem. Commun.* **2020**, *56*, 8289–8292.
- [63] B. Jouvet, B. Isare, L. Bouteiller, P. van der Schoot, *Langmuir* **2014**, *30*, 4570–4575.
- [64] a) J. V. Selinger, M. S. Spector, J. M. Schnur, *J. Phys. Chem.* **2001**, *105*, 7157–7169; b) T. G. Barclay, K. Constantopoulos, J. Matison, *Chem. Rev.* **2014**, *114*, 10217–10291; c) A. Brizard, R. Oda, I. Huc, *Top. Curr. Chem.* **2005**, *256*, 167–218.
- [65] a) M. Liu, L. Zhang, T. Wang, *Chem. Rev.* **2015**, *115*, 7304–7397; b) G. Liu, C. Zhou, W. L. Teo, Ch. Qian, Y. Zhao, *Angew. Chem. Int. Ed.* **2019**, *58*, 9366–9372; *Angew. Chem.* **2019**, *131*, 9466–9472; c) S. Yu, R. Sun, T. Chen, L. Y. Jin, *Soft Matter* **2018**, *14*, 6822–6827.
- [66] a) Z. Shen, T. Wang, M. Liu, *Angew. Chem. Int. Ed.* **2014**, *53*, 13424–13428; *Angew. Chem.* **2014**, *126*, 13642–13646; b) L. Zhang, T. Wang, Z. Dhen, M. Liu, *Adv. Mater.* **2016**, *28*, 1044–1059.
- [67] D. de las Heras, J. M. Tavares, M. M. Telo da Gama, *Soft Matter* **2011**, *7*, 5615–5626.
- [68] a) P. Gallo, K. Amann-Winkel, C. A. Angell, M. A. Anisimov, F. Caupin, C. Chakravarty, E. Lascaris, T. Loerting, A. Z. Panagiotopoulos, J. Russo, J. A. Sellberg, H. E. Stanley, H. Tanaka, C. Vega, L. Xu, L. G. M. Pettersson, *Chem. Rev.* **2016**, *116*, 7463–7500; b) L. Longa, M. Ciesla, H.-R. Trebin, *Phys. Rev. E* **2003**, *67*, 061705.
- [69] a) D. M. Hall, G. M. Grason, *Interface Focus* **2017**, *7*, 20160140; b) G. M. Grason, *J. Chem. Phys.* **2016**, *145*, 110901; c) C. J. Forman, S. N. Fejer, D. Chakrabarti, P. D. Barker, D. J. Wales, *J. Phys. Chem. B* **2013**, *117*, 7918–7928.
- [70] V. Corradi, B. I. Sejdiu, H. Mesa-Galloso, H. Abdizadeh, S. Yu, Noskov, S. J. Marrink, D. P. Tieleman, *Chem. Rev.* **2019**, *119*, 5775–5848.
- [71] a) O. Henrich, K. Stratford, M. E. Cates, D. Marenduzzo, *Phys. Rev. Lett.* **2011**, *106*, 107801; b) S. S. Gandhi, L.-C. Chien, *Adv. Mater.* **2017**, *29*, 1704296; A. Yoshizawa, *RSC Adv.* **2013**, *3*, 25475–25497.
- [72] Z.-G. Zheng, Y.-Q. Lu, Q. Li, *Adv. Mater.* **2020**, *32*, 1905318; H. K. Bisoyi, T. J. Bunning, Q. Li, *Adv. Mater.* **2018**, *30*, 1706512.
- [73] In this context it is noted that polar substituents like F and CN in the center of the rod-like cores of symmetric tetracatenars have been reported to inhibit any cubic phase formation and replace it by lamellar phases, see ref. [74].
- [74] A. I. Smirnova, B. Heinrich, B. Donnio, D. W. Bruce, *RSC Adv.* **2015**, *5*, 75149–75159.
- [75] A. R. A. Palmans, E. W. Meijer, *Angew. Chem. Int. Ed.* **2007**, *46*, 8948–8968; *Angew. Chem.* **2007**, *119*, 9106–9126; C. Kulkarni, E. W. Meijer, A. R. A. Palmans, *Acc. Chem. Res.* **2017**, *50*, 1928–1936.
- [76] S. P. Sreenilayam, Y. P. Panarin, J. K. Vij, V. P. Panov, A. Lehmann, M. Poppe, M. Prehm, C. Tschierske, *Nat. Commun.* **2016**, *7*, 11369; M. Poppe, M. Alaasar, A. Lehmann, S. Poppe, M.-G. Tamba, M. Kurachkina, A. Eremin, M. Nagaraj, J. K. Vij, X. Cai, F. Liu, C. Tschierske, *J. Mater. Chem. C* **2020**, *8*, 3316–3336; A. Lehmann, M. Alaasar, M. Poppe, S. Poppe, M. Prehm, M. Nagaraj, S. P. Sreenilayam, Y. P. Panarin, J. K. Vij, C. Tschierske, *Chem. Eur. J.* **2020**, *26*, 4714–4733.
- [77] D. Chen, Y. Shen, J. Agüero, E. Korblova, D. M. Walba, N. Kapernaum, F. Giesselmann, J. Watanabe, J. E. MacLennan, M. A. Glaser, N. A. Clark, *ChemPhysChem* **2014**, *15*, 1502–1507.
- [78] H. Takezoe in *Topics in Current Chemistry Vol. 318* (Ed.: C. Tschierske), Springer, Berlin, **2011**, pp. 303–330.
- [79] K. V. Le, H. Takezoe, F. Araoka, *Adv. Mater.* **2017**, *29*, 1602737.
- [80] a) J. A. Bollinger, T. M. Truskett, *J. Chem. Phys.* **2016**, *145*, 064902; b) M. B. Sweatman, R. Fartaria, L. Lue, *J. Chem. Phys.* **2014**, *140*, 124508; c) C. A. Angell, Z. Zhao, *Faraday Discuss.* **2013**, *167*, 625–641; d) H. Tanaka, *Eur. Phys. J. E* **2012**, *35*, 113; e) T. S. Ingebrigtsen, T. B. Schröder, J. C. Dyre, *Phys. Rev. X* **2012**, *2*, 011011.

Manuscript received: June 14, 2020

Accepted manuscript online: July 11, 2020

Version of record online: October 29, 2020